Axial Motion Correction Using Piezo-Controlled Synchronization for Two-Photon Microscopy

Macy Mora-Antoinette and Karl J Lewis
Cornell University

Abstract

Here, we augment a novel approach previously reported by our lab to improve image capture of calcium dynamics in osteocytes in vivo. This device allows for imaging of whole bone during mechanical loading and could be useful to anyone seeking to understand osteocyte mechanobiology. The synchronization system we develop here allows for the communication of and synchronication of two distinct piezo devices using the analog inputs/outputs of their respective controllers. One piezo actuator is responsible for applying mechanical loads to the bone, while the other controls the movement of the microscope's objective. Using this technique, we ensure that the objective follows the small axial displacements of the bone to avoid introducing significant motion artifacts. By minimizing motion artifacts during in vivo imaging, we more accurately assess the biological response of bone cells to mechanical stress, offering new insights into bone physiology and mechanotransduction.

1. Introduction

In vivo two-photon microscopy has revolutionized the way biological tissues are studied, particularly for applications in neuroscience, developmental biology, and, more recently, bone imaging[1–3]. The ability to capture high-resolution fluorescence data deep within living tissue provides unique insights into cellular dynamics and tissue physiology. However, as with many imaging modalities, intravital two-photon imaging is highly susceptible to motion artifacts, particularly in the axial direction. These artifacts can significantly distort the data by introducing false changes in fluorescence intensity that may be erroneously interpreted as biological responses. Axial motion artifacts are especially problematic in tissues that experience mechanical deformation during imaging, such as the brain during head movements or the heart during the cardiac cycle. As we will show here, even a hard tissue like bone is no exception. Numerous research groups have attempted to address these challenges through various motion-correction methods, but a universal solution has yet to be found.

Motion correction techniques for two-photon microscopy have often focused on compensating for lateral movement, particularly in the brain. One common approach is to use post-processing algorithms, which have shown some success in stabilizing imaging volumes but are limited when it comes to axial movement. For example, in studies involving simultaneous multi-plane two-photon calcium imaging, axial motion introduces challenges that cannot easily be corrected with post-processing because changes in fluorescence intensity are indistinguishable from neural activity-induced fluctuations [4]. Another study describes an automated correction method for fast motion artifacts in two-photon imaging of awake animals [5]. Their work emphasizes the challenges of imaging dynamic tissues, particularly in the brain, where displacements can introduce non-uniform distortions in the scanned images. Some research groups have experimented with two-color labeling techniques for motion correction in small axial displacements [6], though this approach is constrained by reduced frame rates and potential phototoxicity. Other team have developed hardware-based solutions involving active tracking of moving samples using reference signals or fiducials, such as fluorescent beads or naturally occurring structures within the tissue [7].

However, these methods come with their own challenges, including the invasiveness of fiducial introduction and the difficulty of tracking naturally occurring fiducials in sparsely populated regions. Another relevant example is the work by Soulet et al., which introduced an adaptive compensation technique for in vivo imaging of fast cellular dynamics. Their method employed a system to track and correct tissue movement in real-time, allowing for more accurate imaging of moving tissues, such as the spinal cord [8].

Despite these advances, axial motion correction remains particularly challenging when imaging mechanically loaded tissues like bone. Bones, unlike soft tissues such as the brain or heart, are rigid and experience smaller degrees of deformation. However, during active mechanical loading, such as compression loading of skeletal long bones,

even small deflections on the micrometer scale can occur. While these deflections may seem negligible, the high axial resolution of two-photon microscopes, often around 0.5 μm, is sufficient to detect them. This introduces motion artifacts that can confound fluorescence measurements, making it difficult to discern whether changes in intensity are due to the biological response of bone cells or simple movement of the region of interest in and out of the focal plane.

Our research addresses this problem by developing a novel motion-correction method tailored to mechanically loaded bone imaging. Here, we use a novel approach previously reported by our lab with the ability to image calcium dynamics in osteocytes in vivo. This device allows for imaging during mechanical loading of whole bone and could be useful to anyone seeking to understand osteocyte mechanobiology [1, 2]. In contrast to previous approaches, which either focus on lateral motion or use fiducials, we employ a piezo-driven controller to synchronize the movements of the two-photon microscope's objective with the mechanical loading of the bone. This synchronization ensures that the focal plane remains aligned with the sample, even as small deflections occur during active mechanical loading. Our system enables precise fluorescence measurements of calcium dynamics in bone cells, even under high strain conditions, where motion artifacts are most pronounced.

The synchronization system we developed uses two separate controllers to operate two distinct piezo devices. One piezo actuator is responsible for applying mechanical loads to the bone, while the other controls the movement of the microscope's objective. By synchronizing the analog signals between these controllers, we can ensure that the objective follows the small displacements of the bone without introducing significant motion artifacts. Importantly, the objective moves only a fraction of the amplitude of the loading actuator, ensuring that even micrometer-level deflections are corrected without overshooting or losing resolution.

This approach represents a significant advancement in the field of bone imaging, particularly for studies involving mechanical loading and calcium signaling. By minimizing motion artifacts during in vivo imaging, we can more accurately assess the biological response of bone cells to mechanical stress, offering new insights into bone physiology and mechanotransduction. Additionally, our system provides a user-friendly, robust framework that can be easily adapted to other mechanically loaded tissues, expanding the utility of two-photon imaging across a variety of biological applications.

2. Methods

All procedures were approved by Cornell University IACUC.

2.1. Static Fluorescent Labeling with Calcein in Mice

Standard female laboratory mice C57BL/6J from JAX were ordered and aged to skeletal maturity. At 16-weeks old, three mice were injected with calcein for static fluorescent labeling of osteocytes. Calcein solution was made with a standard recipe of 0.12 calcien (Sigma; 154071-48-4) and 0.05 sodium bicarbonate in 25mL of 1x PBS. Solution was filtered for sterility under vacuum using a millapore filter (Sigma; SCGP00525). 200uL were injected intraperitoneally into each mouse. 1-3 hours after injection, mice were imaged under two-photon microscopy. Osteocytes were visibly labeled with strong calcein signal.

2.2. Dynamic Fluorescent labeling with osteocyte-targeted GCaMP in mice

Mice exhibiting osteocyte-targeted expression of GCaMP6f were achieved by crossing Ai38 mice B6J.CgGt(ROSA)26Sortm95.1(CAGGCaMP6f)Hze/MwarJ (JAX Labs, strain no. 028865), which contain GCaMP6f DNA behind a Lox-STOP-Lox codon [9], with DMP1-Cre mice [B6N.FVB-Tg(Dmp1-cre)1Jqfe/ BwdJ; (JAX Labs, strain no. 023047) [10]. Mice were then bred onto a C57BL/6 background. GCaMP6f is a recombinant protein construct containing calmodulin (CaM), the CaM binding myosin light chain kinase fragment (M13), and enhanced green fluorescent protein (EGFP). Bright EGFP fluorescence is observed following Ca2+ binding to CaM, causing a subsequent binding of CaM to M13 and a conformational change that results in increased fluorescence intensity. Previous studies with this mouse model used GCaMP3 and validated fluorescent expression in cortical osteocytes [11]. Our substitution with GCaMP6f was motivated by the fact that GCaMP6f in particular was created as an ultrasensitive protein calcium sensor that outperforms alternative GCaMPs with a variant that has faster kinetics and greater dynamic range [9].

2.3. Calibrations for mice

Before loading, calibrations were conducted with digital image correlation (DIC) to determine position-controlled loading regimes with corresponding strain values. Hind paws from 3-6 mice for each of the mouse groups were amputated and stored in saline soaked gauze at -20oC until calibration. For calibration, paws were thawed at room temperature in DPBS. The MT3 was surgically isolated as described elsewhere [2] and a 100 μm diameter cylindrical fulcrum pin was inserted just underneath, separating the bone from any muscle fascia and soft tissue. A bracket for the two side pins was then positioned over the foot and connected with a screw to the load cell and actuator. A stepladder loading regime under compression was applied with 2 second intervals holding load constant and 5μm in-

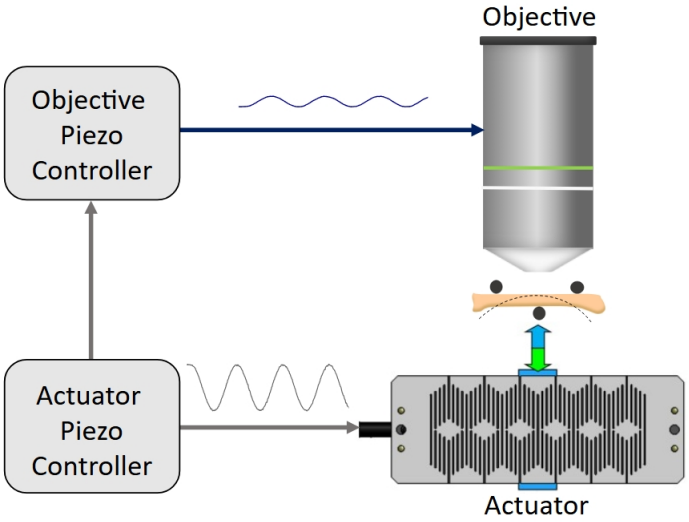

(a) Experimental Setup

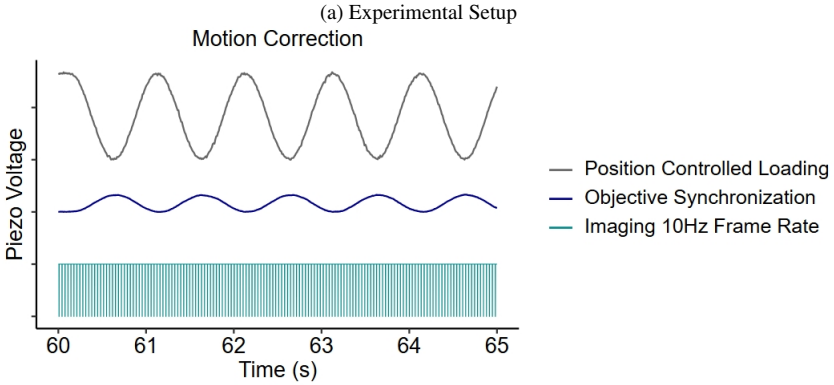

(b) Analog Output/Input Signals

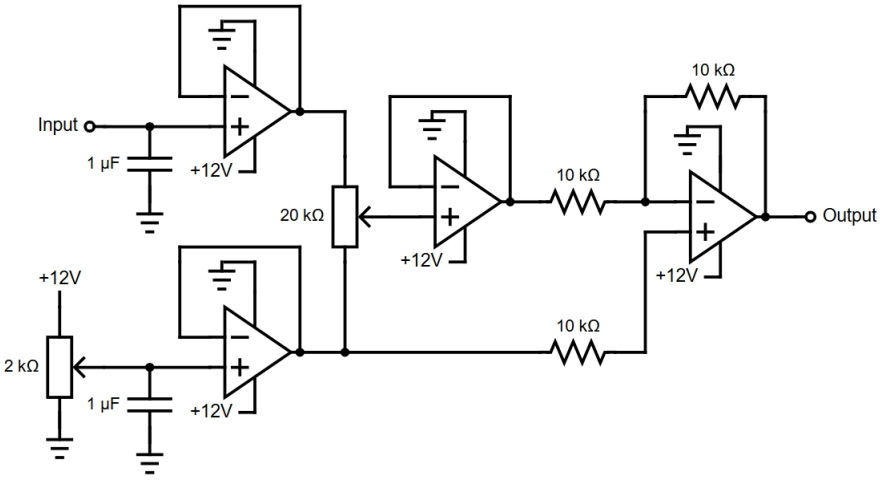

(c) Circuit

Figure 1. Motion artifact correction. A diagram showing how we take a second piezoelectric controller that can move the objective in synchrony with the loading. The amplitude is reduced with a user-defined variable resistance using a potentiometer. This synchronizes the objective movement with small displacements level with that of the small deflections on the bone during compressive loading. (Top) The circuit diagram created in order to connect the two controllers for both the loading actuator and the objective. The input is the signal to directly control the loading actuator. The output is the user defined reduction of the signal for the objective. (Bottom) Data collected from the ThorSynch software showing the piezo voltages of the different signals, including the input (loading device), output (objective), and frame acquisition.

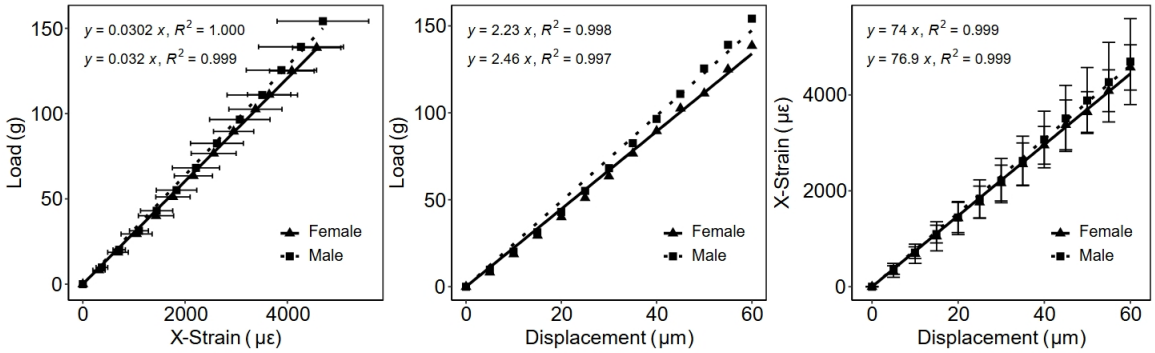

Figure 2. Calibrations for Female and Male GCaMP6f mice. For calibrations, linear regressions were conducted using R (v.3.6) for each group with a controlled intercept through the origin. Regressions were made with X- strain vs displacement as well as X-strain vs load to compute applied displacement values for position-controlled loading and the expected average max load.

cremental steps until reaching 60μm displacement before releasing the load in the same pattern but in reverse. For DIC, 26μm diameter Fluoresbrite YG Microspheres (Polysciences 18241-2) were applied and bound onto the MT3 cortex. Images were taken during loading with a 10x objective at 30 fps with 410nm epifluorescence and optics from the two-photon Bergamo II microscope (Thor Labs). Changes in displacements of the beads were computed in MATLAB to determine strain values on the surface of the bone.

2.4. In vivo loading of the third metatarsal

Mouse third metatarsals (MT3) were surgically exposed and placed into a custom made stainless steel in vivo three-point bending device as previously described [1, 2]. For experiments, mice were initially placed under anesthesia in a small container with 1L/min flow rate and 3% isoflurane. Mice were then transferred onto the loading device stage with a heating pad and head covering for more direct anesthesia, where the isoflurane was reduced to 2%, at which point surgery in the same manner as with calibration took place on the left hind paw. With a live mouse, it was now important to avoid rupture of blood vessels and to remove any tendon that resides longitudinally across the metatarsals. The fulcrum pin and bracket are attached accordingly. The paw is placed in a room temperature DPBS bath for the duration of the experiment. 1 Hz cyclic haversine position-controlled loading was applied for 60 seconds to previously calibrated peak strains of 1000, 2000 and 3000$\mu\varepsilon$. These levels encompass the range of strains that have reported during physiological activities from in vivo strain gage studies, with strains up to 2000$\mu\varepsilon$ characteristic of habitual activities, while strains on the order of 3000$\mu\varepsilon$ are seen in extreme activities [12, 13].

2.5. Intravital imaging with two-photon microscopy

In vivo static and dynamic fluorescence signals were visualized with a two-photon microscope (Thor Labs Bergamo II; Newton, NJ) and a 20x water immersion objective with a long working distance (XLUMPLFLN, Olympus). Osteocytes were imaged at the dorsal mid-shaft region of the MT3, directly above where the fulcrum pin was placed beneath the bone, and beneath the periosteal surface, verified with visible autofluorescence from the bone surface. The ROI was 512 x 512 pixels with 2x zoom, leading to a pixel size of 0.545 x 0.545 μm. Excitation was at 920 nm wavelength from a tunable Ti-Saphire laser (Coherent Chameleon Discovery NX). For calcein labeling, the power selected was such that the final output from the objective was between 10 mW and a PMT with a 490-560 nm bandpass filter was used for detection with a voltage gain of 0.6 V. For GCaMP labeling, the power was between 30-35 mW and a PMT voltage gain of 0.7 V. Time series images were acquired by averaging 3 frames with a sampling rate of 29.4Hz, leading to final frame rate of 9.8 fps. Across an approximate 150 second period, 1500 8-bit TIF images were collected, with 60 seconds non-loading, 60 seconds loading, and 30 seconds resting.

2.6. Correcting motion artifacts at high loading displacements

Motion artifacts during imaging of living animals is not uncommon in biological research. In the case of active mechanical loading, even compression loading on a skeletal long-bone, which is asymmetric in shape without a smooth surface for load application, small strain level deflections may be possible. The deflections are on the order of micrometers, and thus may be negligible at the mathematical level and even unseen to the human eye. However, a two-

photon microscope may have a Z-resolution approximately 0.5 μm in size and is thus able to capture these small displacements. The result is an axial motion artifact, with the ROI moving in and out of plane. For small displacements at lower magnitude strains (1000 $\mu\varepsilon$ and below), this is generally not an issue. However, for strain magnitudes representing high physical activity (2000-3000 $\mu\varepsilon$), there may be small deflections. In and out of plane motion may cause dramatic increases to the cell's fluorescence intensity amplitude, confounding whether the signal captured by the optics is due to motion artifact or a true biological response.

To improve the current simultaneous MT3 loading and imaging setup, this chapter creates a more robust data acquisition protocol of Ca2+ dynamics at higher applied displacements. We have created a user-friendly system that allows for synchronization of the objective movements with the position-controlled loading regime (Figure 1). This technique requires the use of two separate controllers (PI E-709.SRG and ThorLabs Precision Controller) that each send voltages to two separate piezo devices, namely, the loading actuator (PI P-602.5SL) and the objective. The controller for the loading actuator can send an analog signal to the same controller for the objective controller, thus both objects will be perfectly synchronized. However, the objective need not move the full amplitude of the loading device, but only a fraction that is on par with the small deflections seen in the bone. Figure 1 shows a circuit diagram connecting the two systems. For the reasons stated above, a potentiometer (20kΩ; Bourns-3590P-2-203L) allows the user to manually increase the resistance and reduce the signal amplitude as needed. A second potentiometer (2kΩ; Bourns-3362P-1-202LF) exists as a second constant input to ensure as the user increases the resistance of the first, the signal will maintain the same average value. Buffered operational amplifiers (op-amps, elements that contain their own power sources) are included to prevent any signal attenuation that may occur throughout the circuit. Grounded capacitors (1μF) at the two inputs are used for fine-tuning by removing high-frequency and low-level noise that might exist in the system. The final op-amp is an inverter (10 kΩ); in particular to our setup, the piezo crystal of the loading actuator happens to be in a reverse orientation than the piezo crystal of the Thor Labs objective. Thus, the displacement mechanisms respond the same with inverted signals. The final two resistors (10 kΩ) in the circuit may be considered to provide safety factors should the circuit ever be short circuited. The op-amps were consolidated using 2 dual-circuit op-amps (Texas Instruments TLV272 Rail-to-Rail). Figure 1 shows data collected from the ThorSynch software showing the piezo voltages of the different signals, including the input (loading device), output (objective), and frame acquisition. The objective axial position is in-phase and inverted, with a user-defined reduction in the amplitude.

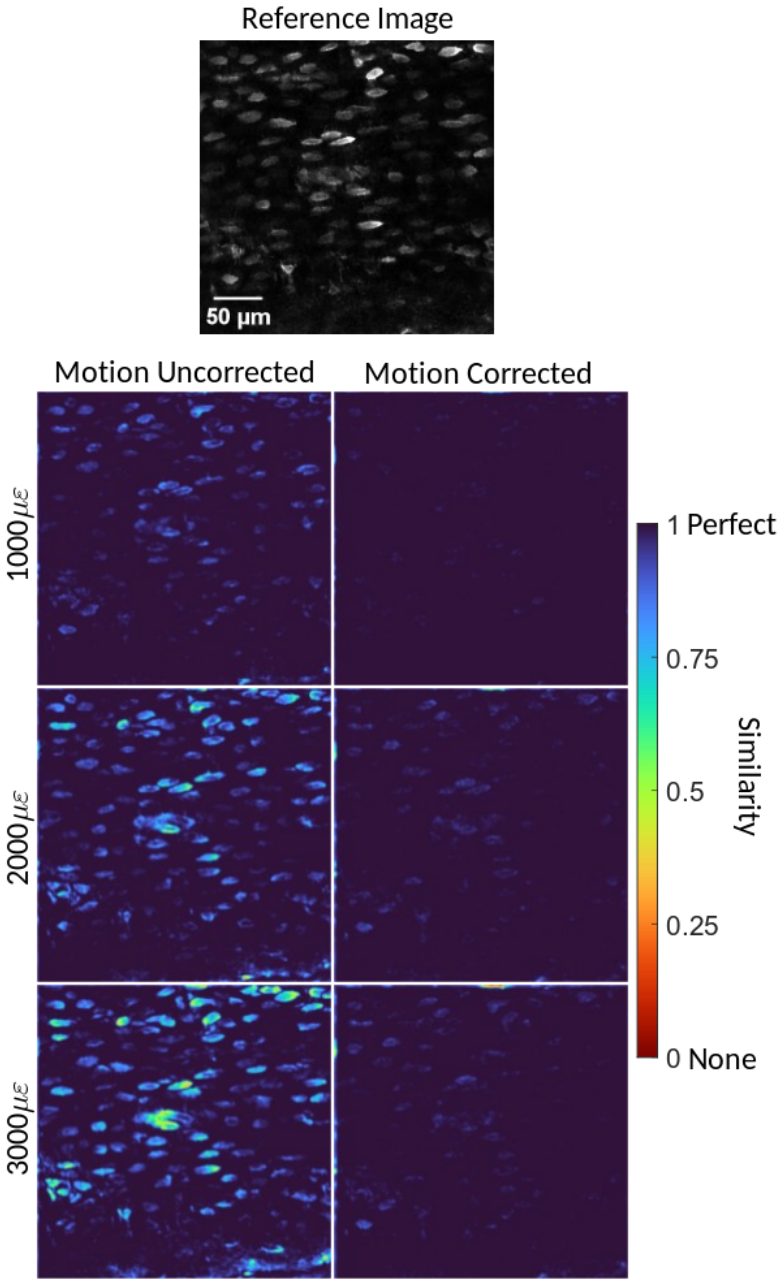

Figure 3. SSIM (similarity between loaded vs nonloaded images) shown as a heatmap in calcein injected mice. Areas with high differences (i.e. low similarity) are visible at 2000us and 3000us. Uncorrected motion is shown on the left and corrected motion is shown on the right. This exemplifies how much change is artificially created when motion is not corrected. Correcting for motion removes these artificial changes. Videos of respective heatmaps are available for metatarsal loading at 1000us (Supplemental Video 1), 2000$\mu\varepsilon$ (Supplemental Video 2) and 3000$\mu\varepsilon$ (Supplemental Video 3).

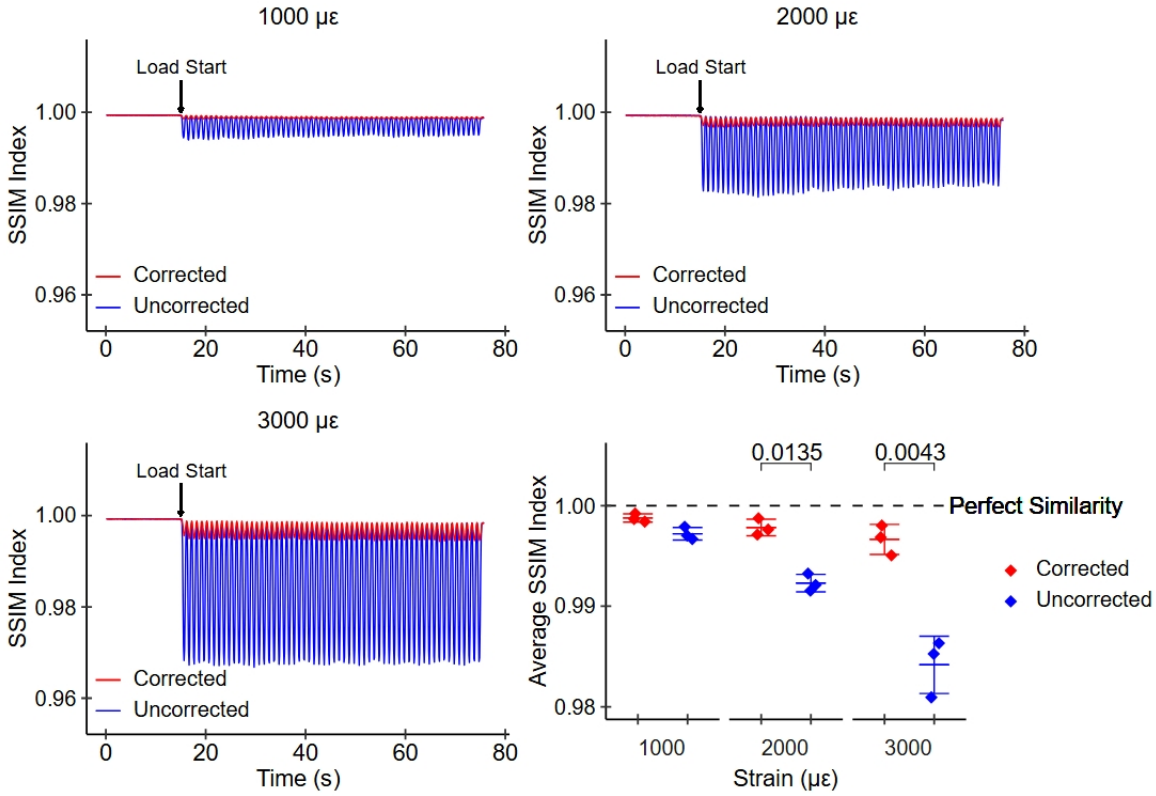

Figure 4. Similarity index) quantified over the 60 second loading period for 1000$\mu\varepsilon$, 2000$\mu\varepsilon$, and 3000$\mu\varepsilon$ with calcein injected mice. When loading reaches maximum displacement, the SSIM correspondingly reduces to indicate a maximum change in similarity from the static reference frame, with 3000$\mu\varepsilon$ showing more pronounced dissimilarity than 2000$\mu\varepsilon$, and 2000$\mu\varepsilon$ showing more than 1000$\mu\varepsilon$. There is a clear cyclical pattern following the pattern of loading. With motion correction from objective synchronization, all significant changes to the frame or focal plane are removed, increasing the similarity to near 1.

2.7. Error Analysis with Structural Similarity Index

The Structural Similarity (SSIM) Index is a method for measuring the similarity between two images. Unlike traditional measures like Mean Squared Error (MSE) or Peak Signal-to-Noise Ratio (PSNR), which consider absolute errors, SSIM is designed to model the human visual system's perception of image quality. Is a weighted combination of the changes in luminance, contrast, and structure. The SSIM index between two images x and y is defined as:

$$\mathrm{SSIM}(x,y) = \frac{(2\mu_x\mu_y + C_1)(2\sigma_{xy} + C_2)}{(\mu_x^2 + \mu_y^2 + C_1)(\sigma_x^2 + \sigma_y^2 + C_2)}, \quad (1)$$

where:

- μ_x and μ_y are the mean intensities of images (or patches) x and y, respectively,
- σ_x^2 and σ_y^2 are the variances of x and y, respectively,
- σ_{xy} is the covariance between x and y,
- C_1 and C_2 are small positive constants introduced to avoid instability when the denominators are close to zero.

SSIM attains its maximum value of 1 when the two images are identical; values closer to 1 indicate greater structural similarity.

Since calcein is a static fluorescent marker, it can be assumed that artificial changes in fluorescence during mechanical loading that cause reductions in image similarity are likely due to motion artifact. Comparing images across a loading cycle to images under a non-loaded reference could therefore be used to determine the prominence of the motion artifact in the system. SSIM was computed in MATLAB.

2.8. Artificial Fluorescent Intensity Analysis

Intensity measurements were performed by post-processing images using Image J. In-plane movements in the x and y were removed using the template matching plugin. ROIs were selected with a semi-automated process. A mask was selected using thresholding selected by the user

after projecting across the z with mean intensity followed by enhancing the contrast and applying a gaussian blur with sigma of 1. Size exclusion was performed, filtering ROIs for only 150-650 pixel sizes. Finally, users would manually make final adjustments to ROIs by eye, deleting and adding ROIs as needed that were not properly capture by thresholding. An ROI indicating the background autofluorescence was included in an area where no cells were present. The average pixel intensity for each ROI was collected across all 1500 time series frames and output as a csv.

In MATLAB, ROIs that exceeded a cutoff of the mean background intensity plus 3 standard deviations were included in the final analysis as fluorescent osteocytes. The intensities for each cell of interest were detrended linearly to correct for photobleaching and normalized to the mean intensity for that cell over a 40 second period prior to loading. Peaks and troughs were identified using islocalmax and islocalmin in MATLAB with a prominence of 0.01. Amplitudes across the non-loaded and loaded intervals were computed by subtracting coupled troughs from peaks. Normalization of fluorescent intensity was computed as follows Fload/Fnon-load with static values Fnon-load/ Fnon-load = 1 being used as reference controls. Fload indicates the amplitude during loading and Fnonload indicates the amplitude without loading. Since calcein is a static fluorescent marker, it can be assumed that artificial changes in fluorescence during mechanical loading are likely due to motion artifact.

2.9. Statistical analysis

The effect of the corrected versus uncorrected motion on the SSIM were determined using a one-way ANOVA with followed by paired one-tailed T-test with alternative hypotheses of uncorrected is greater than the corrected group. Changes in normalized artificial fluorescence were determined by were determined using a two-way ANOVA with by paired one-tailed T-test with alternative hypotheses that fluorescence during uncorrected and corrected loading are greater than the static reference group. Statistical tests were conducted using R (v.3.6) with $\alpha = 0.05$.

3. Results

3.1. Calibrations for male and female GCaMP6f mice

In order to determine the necessary displacements required to reach physiological strain values spanning the range of 1000-3000$\mu\varepsilon$, calibrations were performed on previously dissected GCaMP6f mouse paws. Linear displacement calibrations are consistent within male and female knockout groups (Figure S1). The max position required for male and female groups to reach a strain value of 3000$\mu\varepsilon$ is near 40 μm with expected average maximum loads to be greater in male mice than female mice (Figure S1). These values are slightly higher than what has been previously reported for GCaMP3 mice [1], and the use of high displacements lead to motion artifacts visible at 2000$\mu\varepsilon$ and 3000$\mu\varepsilon$. This motivated the need to create a motion artifact correction system that was previously not as prominent an issue in prior experiments.

3.2. Successful removal of motion artifacts allow for higher loading displacements

In order to determine if motion artifact is successfully removed while loading at higher displacements, we use a static fluorescent marker, calcein, for reference. As a static marker, changes in the fluorescent intensity during loading are likely due to axial motion artifact. These would be considered artificial fluorescent changes. Mice were injected with calcein intraperitoneally and imaged 1-3 hours later with metatarsal loading at 1000us (Supplemental Video 1), 2000$\mu\varepsilon$ (Supplemental Video 2) and 3000$\mu\varepsilon$ (Supplemental Video 3). Images were captured both with and without motion correction.

The synchronization of the objective with the loading regime successfully removed the motion artifact seen at higher load displacements. Figure 3 shows a representative ROI in a mouse with changes in SSIM visible when moving through a loading cycle. Without the corrected objective synchronization, there is visible motion artifact in the z-plane, causing the ROI to change over the duration of a single loading cycle. However, with the objective synchronized using the user-defined signal reduction of the position-controlled loading regime, little to no changes are visible in the ROI. This allows for successful capturing of robust calcium dynamics without the confounding issue that the in and out of plane movement may lead to false positive results regarding the biological response of the cells. Figure 4 quantifies the SSIM over the 60 second loading period. Figure 4 shows that as loading reaches maximum displacement, the SSIM correspondingly reduces to indicate a maximum change in similarity from the static reference frame, with 3000$\mu\varepsilon$ showing more pronounced dissimilarity than 2000$\mu\varepsilon$, and 2000$\mu\varepsilon$ showing more than 1000$\mu\varepsilon$. With motion correction from objective synchronization, all significant changes to the frame (i.e. the focal plane) are removed (Figure 4).

Finally, we decided to quantify the artificially changes in fluorescence that may be produced if axial motion is not properly corrected. Figure 5 shows the fluorescence that may be wrongfully determined as a biological response is seen with a dynamic fluorescent marker such as GCaMP6f, but is really produced by the changing focal plane. At 1000$\mu\varepsilon$, the uncorrected motion reduces from 100% change in fluorescence when compared to the 40 second non-loaded reference period. At 2000$\mu\varepsilon$, the uncorrected motion re-

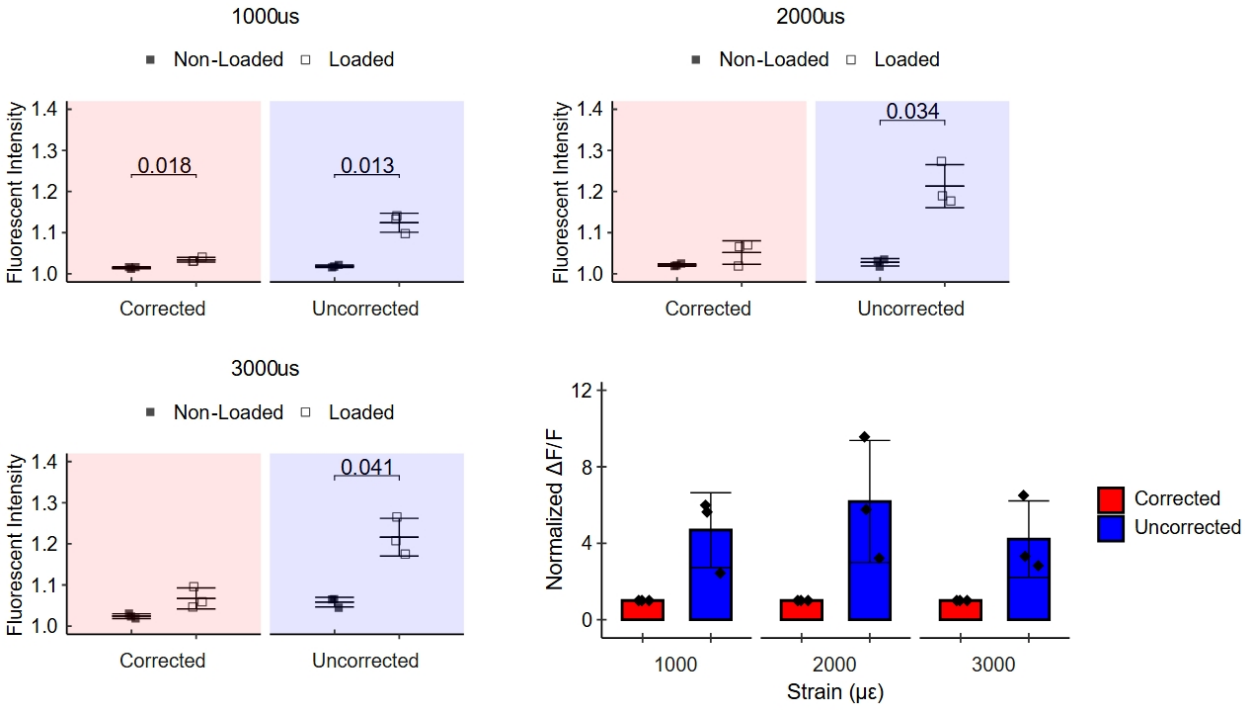

Figure 5. Fluorescent intensity F in calcein injected mice showing just an artificial increase in intensity during loading at 1000$\mu\varepsilon$, 2000$\mu\varepsilon$, and 3000$\mu\varepsilon$. Correcting for motion removes all significant changes. When computing ΔF/F for corrected and uncorrected motion, and normalizing the uncorrected ΔF/F by the corrected ΔF/F, we can see drastic artificial increases in fluorescence in comparison when motion is not corrected.

duces from 100% to only 10% change in fluorescence. At 3000$\mu\varepsilon$, the uncorrected motion reduces from 100% to only 10% change in fluorescence. These reductions are very significant and indicate that our system can correct for up to 100% artificial fluorescent changes created by motion artifact. When we compute the ΔF/F for corrected and uncorrected motion, and we normalize the uncorrected ΔF/F by the corrected ΔF/F, we can see drastic artificial increases in fluorescence that are corrected (Figure 5).

3.3. Robust Calcium Signals are collected with GCaMP mice

Now that motion artifacts are removed from the system, it is possible to capture robust calcium signals. We validated this by performing MT3 loading on GCaMP6f mice. Figure 6 shows the response of a single cell (i.e. osteocyte) from a skeletally mature male GCaMP6f with the corresponding displacement and loads at each frame.

4. Discussion

It is difficult to study osteocytes experimentally because of their embedded position in the hard tissue matrix, to which they rapidly deteriorate or dedifferentiate upon removal of this niche. Here, we use a novel technique capable of imaging osteocytes intravitally and during active loading and movement of the bone [1, 2]. Osteocyte mechanotransduction in vivo is highly dependent on their immediate microenvironment. Matrix-binding proteins (e.g., proteoglycans, integrins) provide functional attachments between osteocyte cell membranes in an arrangement that is critical for fluid activation of the cell [14, 15]. In addition, there are a multitude of channels and receptors that are involved in Ca2+ signaling of osteocytes [16].

Ongoing development of the in vivo MT3 loading and imaging approach includes the use of multiple markers with different fluorescence emission properties to label both structural and functional activity. The Structural Similarity (SSIM) Index is used as a form or error analysis to quantify how our system has been improved. SSIM is a method for measuring the similarity between two images. Unlike traditional measures like Mean Squared Error (MSE) or Peak Signal-to-Noise Ratio (PSNR), which consider absolute errors, SSIM is designed to model the human visual system's perception of image quality. Is a weighted combination of the changes in luminance, contrast, and structure.

The synchronization system we developed uses two

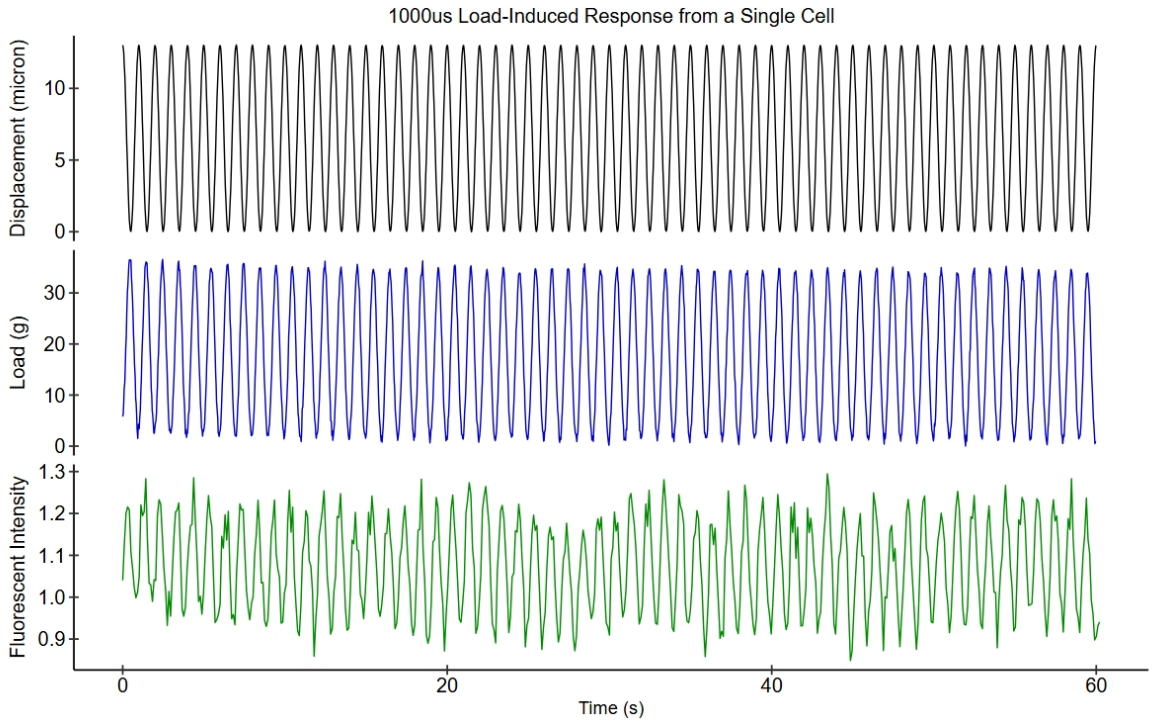

Figure 6. Example Response from a single cell in a GCaMP6f mouse with robust calcium signaling capture.

separate controllers to operate two distinct piezo devices. One piezo actuator is responsible for applying mechanical loads to the bone, while the other controls the movement of the microscope's objective. By synchronizing the analog signals between these controllers, we can ensure that the objective follows the small displacements of the bone without introducing significant motion artifacts. Importantly, the objective moves only a fraction of the amplitude of the loading actuator, ensuring that even micrometer-level deflections are corrected without overshooting or losing resolution.

This approach represents a significant advancement in the field of bone imaging, particularly for studies involving mechanical loading and calcium signaling. By minimizing motion artifacts during in vivo imaging, we can more accurately assess the biological response of bone cells to mechanical stress, offering new insights into bone physiology and mechanotransduction. Additionally, our system provides a user-friendly, robust framework that can be easily adapted to other mechanically loaded tissues, expanding the utility of two-photon imaging across a variety of biological applications.

5. Supplemental Material

Supplemental Video 1
Supplemental Video 2
Supplemental Video 3

6. Acknowledgements

We thank Karly Hooper for maintaining mouse colonies for use in these experiments, along with the entire CARE staff in Weill Hall. We also thank Daniel Rivera for assistance with the design and troubleshooting of the motion correction circuitry. This work was supported by the Department of Biomedical Engineering at Cornell University, the Mong Family Foundation at Cornell University, and the Ford Foundation by the National Academies of Sciences, Medicine, and Engineering, NIH S10OD023466.

7. References

1. Lewis KJ, Frikha-Benayed D, Louie J, Stephen S, Spray DC, Thi MM, Seref-Ferlengez Z, Majeska RJ, Weinbaum S, Schaffler MB (2017). Osteocyte calcium signals encode strain magnitude and loading frequency *in vivo*. *Proc Natl Acad Sci USA*, 114:11775–11780.

2. Lewis KJ, Boorman-Padgett JF, Castaneda M, Spray DC, Thi MM, Schaffler MB (2023). A fluorescent intravital imaging approach to study load-induced calcium signaling dynamics in mouse osteocytes. *Journal of Visualized Experiments (JoVE)*, 64366.

3. Svoboda K, Yasuda R (2006). Principles of two-photon excitation microscopy and its applications to neuroscience. *Neuron*, 50:823–839.

4. Flores-Valle A, Seelig JD (2022). Axial motion estimation and correction for simultaneous multi-plane two-photon calcium imaging. *Biomedical Optics Express*, 13:2035.

5. Greenberg DS, Kerr JND (2009). Automated correction of fast motion artifacts for two-photon imaging of awake animals. *Journal of Neuroscience Methods*, 176:1–15.

6. Ryan TM, Hinojosa AJ, Vroman R, Papasavvas C, Lagnado L (2020). Correction of z-motion artefacts to allow population imaging of synaptic activity in behaving mice. *The Journal of Physiology*, 598:1809–1827.

7. Aghayee S, Winkowski DE, Bowen Z, Marshall EE, Harrington MJ, Kanold PO, Losert W (2017). Particle tracking facilitates real-time capable motion correction in 2D or 3D two-photon imaging of neuronal activity. *Frontiers in Neural Circuits*, 11:56.

8. Soulet D, Paré A, Coste J, Lacroix S (2013). Automated filtering of intrinsic movement artifacts during two-photon intravital microscopy. *PLoS ONE*, 8:e53942.

9. Chen T-W, Wardill TJ, Sun Y, Pulver SR, Renninger SL, Baohan A, Schreiter ER, Kerr RA, Orger MB, Jayaraman V, Looger LL, Svoboda K, Kim DS (2013). Ultrasensitive fluorescent proteins for imaging neuronal activity. *Nature*, 499:295–300.

10. Lu Y, Xie Y, Zhang S, Dusevich V, Bonewald LF, Feng JQ (2007). DMP1-targeted Cre expression in odontoblasts and osteocytes. *Journal of Dental Research*, 86:320–325.

11. Lewis KJ (2021). Osteocyte calcium signaling – a potential translator of mechanical load to mechanobiology. *Bone*, 153:116136.

12. Rubin CT, Lanyon LE (1984). Dynamic strain similarity in vertebrates; an alternative to allometric limb bone scaling. *Journal of Theoretical Biology*, 107:321–327.

13. Burr DB, Milgrom C, Fyhrie D, Forwood M, Nyska M, Finestone A, Hoshaw S, Saiag E, Simkin A (1996). In vivo measurement of human tibial strains during vigorous activity. *Bone*, 18:405–410.

14. McNamara LM, Majeska RJ, Weinbaum S, Friedrich V, Schaffler MB (2009). Attachment of osteocyte cell processes to the bone matrix. *Anatomical Record*, 292:355–363.

15. Wang Y, McNamara LM, Schaffler MB, Weinbaum S (2007). A model for the role of integrins in flow-induced mechanotransduction in osteocytes. *Proc Natl Acad Sci USA*, 104:15941–15946.

16. Qin L, Liu W, Cao H, Xiao G (2020). Molecular mechanosensors in osteocytes. *Bone Research*, 8:23.